Joint Special Interest Group meeting between euspen and ASPE
Advancing Precision in Additive Manufacturing
Ecole Centrale de Nantes, France, September 2019
www.euspen.eu

Considerations for interpreting in-situ photodiode sensor data in pulsed mode laser powder bed fusion

Venkata Karthik Nadipalli[1], Sebastian A. Andersen[1], Jakob S. Nielsen[1], David B. Pedersen[1]

[1]*Department of Mechanical Engineering, Technical University of Denmark*

vkna@mek.dtu.dk

Abstract
Meltpool emissions across the visible and infrared spectrum are typically used to monitor the quality of laser welds. Laser powder bed fusion (L-PBF) is essentially laser welding on a powder bed. Hence, several commercially available L-PBF systems are equipped with photo sensors installed in co-axial and off-axial orientations. In-situ sensor data is often treated as a proxy for part quality to be used for certification. However, several considerations like design of sensor setup, laser source, material, thermal lensing, etc. can largely vary the quality metrics for anomaly detection. Compared to continuous wave (CW), pulsed mode L-PBF has advantages in manufacturing thin and complex shaped features. In this study, an in-situ photodiode based co-axial and off-axial sensor setup was designed and installed on an open-architecture pulsed mode L-PBF system. The sensor module acquires the real encoder position of the galvo mirrors thus allowing the conversion of time series data into spatial coordinates. The co-axial sensor was found to be very sensitive to alignment, positional dependence, thermal lensing, filters and area of focus. The off-axial sensor is more robust in defect identification. A set of single-track samples were made at varying duty cycles, power levels and speeds. The analysis of the photodiode data showed that anomaly detection in pulsed L-PBF is different than in CW mode of operation. The current study lays the groundwork for a certification of pulsed mode L-PBF components.

Keywords: laser power bed fusion, photodiode sensors, line energy density, single-tracks

1. Introduction

Pulsed laser powder bed fusion (L-PBF) allows for a precise control of heat input thereby enabling the manufacture of thin and complex features. Pulse width modulation can be used in conjunction with in-situ sensors to achieve real time feedback control. Everton et al. and Grasso et al. have reviewed various in-situ sensors for L-PBF. The in-situ sensors can broadly be divided into acoustic, optical, co-axial and off-axial systems as evidenced also from laser welding literature [3]. Acoustic sensors are tough to calibrate, as they are prone to structural noise. Hence, the most commonly used sensors are photodiodes and high-speed cameras across the wavelength spectrum. Craeghs et al. (2010 - 2012), and Clijsters et al. developed a co-axial meltpool monitoring system for L-PBF using a visible camera and a near infrared (NIR) photodiode. Their system uses reflective dichroic mirrors. Demir et al. (2018 - 2019), developed a co-axial meltpool monitoring system with transmittive beam splitters and a set of focussed optics to control the area under inspection. It is critical to control the area of focus to improve the resolution around the meltpool. There is large body of research on using off-axial photo sensors in laser welding and L-PBF [3, 9]. Several commercially available L-PBF systems now offer in-situ sensor modules but the closed black box nature of these systems makes it difficult to develop quality metrics. The following work aims to shine light on the various considerations for design and interpretation of high-speed photo sensor data during L-PBF within an open architecture framework.

2. Experimental setup

The basic experimental setup includes; a custom single layer experimental powder handling unit, a F-θ scan lens (Thorlabs FTH254-1064), a galvanometer (Thorlabs GVS012) as scan head with dielectric coated mirrors, and a 250 W continuous wave fibre laser (SPI SP-250C-W-HS-S-06-QCS) with a wavelength of 1070 nm. A custom-built galvanometer and laser controller was used to vary scan speed, power and duty cycle.

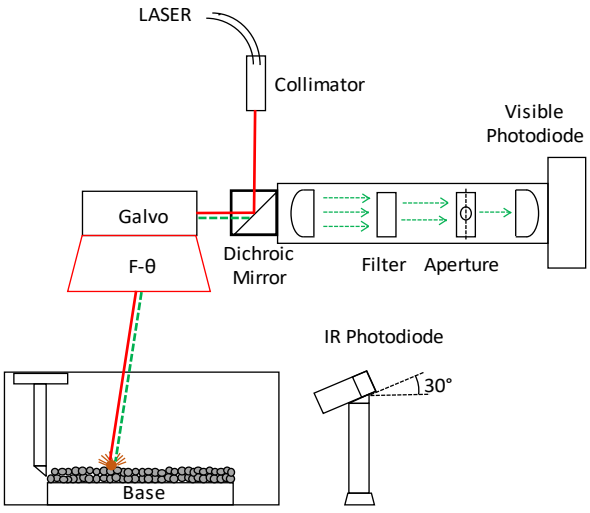

Figure 1. Schematic of open L-PBF system with photodiode sensors

The figure 1 above shows the schematic of the sensor setup. A reflective dichroic mirror (DMSP1000, Thorlabs) was placed in the path of the laser. The dichroic mirror reflects all light above 1000 nm, and transmits light below 950 nm. During L-PBF processing, visible light emitted from the meltpool travels back through the F-θ lens, the galvo mirrors and the dichroic mirror into the co-axial sensor setup. The reflected light first encounters an achromatic doublet (AC254-500-AB, Thorlabs)

focussed at the bottom of the optical path. Thereafter, the light passes through a short or band pass filters. Then, a variable aperture changes the field of view. Finally, the light passes through an achromatic doublet focus lens (AC254-050-AB, Thorlabs) onto a switchable gain Si-based photo detector (PDA36A2 13mm^2 active area) rated from 400 - 1100 nm. The off-axial infrared (IR) sensor is a Ge amplified photo detector (PDA50B2) and has a low pass filter (DMLP1180) which allows light between 1200 - 1800 nm. It is placed at a 30° angle such that the field of view includes the entire 50 mm x 50 mm powder bed. The signals from the two photodiodes along with galvanometer motor encoders, are acquired using an NI C series I/O module with flex logger software. The data acquisition was at 100 kHz frequency providing a fine spatial and temporal resolution.

3. Methodology

3.1. Calibration

The XY location of the laser beam within the powder bed is determined by the angular position of the two galvo mirrors. The F-θ distortion is low in a 50 mm x 50 mm powder bed and was accounted for. After processing a layer, the stored data is analysed in MATLAB to convert the temporal intensity data into a spatial intensity map. The access to the raw data due to the open architecture of our system allows for an in-depth analysis beyond an average intensity value. The figure 2 below shows the laser etching of the DTU logo on the left and a reconstructed intensity map from the IR sensor on the right. The plate made of SS304 had few scratches before etching which resulted in defects within the etching. The reconstructed photodiode image shows the same features as observed in the physical component. There is however, an expected positional dependence of the IR signals from one side to the other. The positional dependence of the off-axial sensor is repeatable and can be corrected.

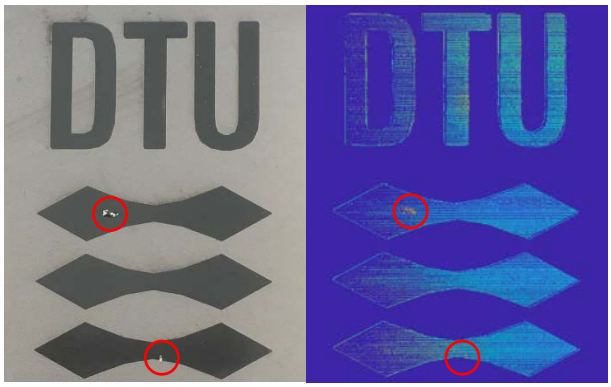

Figure 2. Laser etching of the DTU logo on the left and the reconstructed photodiode image on the right

The co-axial sensor was found to be very sensitive to alignment, positional dependence, thermal lensing, filters and area of focus. In most cases, the sensor behaviour could be repeated even through a change in material, energy density and mode of operation. An example is presented below in Figure 3. Single-track lines were made on mild steel and stainless steel plates at varying power levels, spanning across 40 mm length and starting at different locations within the powder bed. The photodiode signals show a clear position dependent peak at the centre of the powder bed. Changing the optics within the path or the laser beam alignment or the size of the aperture altered the location and the intensity of the peak. Existing literature using reflective optics from Clijsters et al. shows the usage of two additional mirrors for alignment and choosing the area of the focus. Using transmittive dichroic optics like Demir et al. is an alternate solution. Further calibration is required within the co-axial sensor setup to draw conclusions from the results.

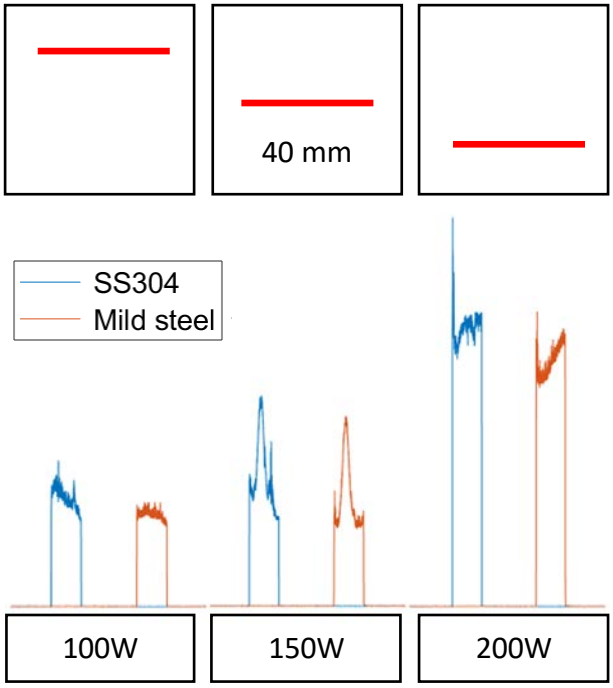

Figure 3. Position dependant trends from co-axial sensor across three power levels and two materials

3.2. Experiments

Single-track samples offer a quick way to analyse a large parameter space and narrow down to an optimal parameter zone. There are several studies in literature exploring single-track samples in CW mode [10] while pulsed mode L-PBF does not have a similar depth in literature. A set of single-track experiments were thus designed to study the effect of laser power, scan speed and duty cycle on off-axial sensor data. The single-track scans also serve as a means to document the effect of pulsing on the meltpool size and shape in L-PBF.

Thirty-two 4 mm long single-tracks of stainless steel 316L powder were manufactured on top of each stainless steel 304 base-plate. Sixteen unique single tracks with four laser powers and four duty cycles with one speed were present on each base-plate. There was a second set of the same single tracks to identify any effect of location and thermal lensing.

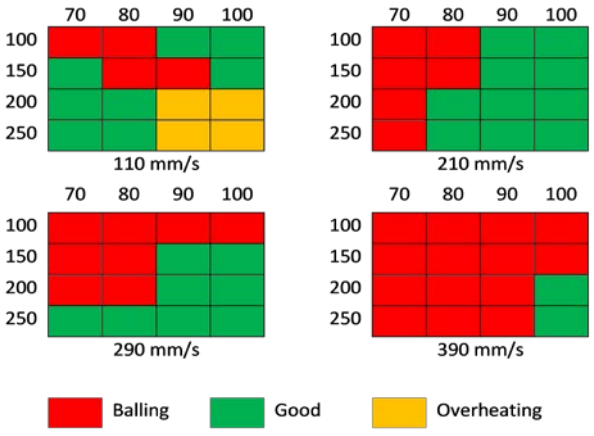

Figure 4. Schematic of single-tracks categorised through visual inspection. Power [W] along Y-axis and duty cycle [%] along X-axis

As shown in figure 4 above the laser power was varied from 100 W to 250 W in increments of 50 W on each base-plate. The duty cycles (%) were 70, 80, 90 and CW. The scan speed was constant in each base-plate and was 110, 210, 290, 390 mm/s across 4 plates. The pulse frequency was chosen to be 1 kHz. The track width of the samples were analysed in a DEMEET optical profilometer that was programmed to identify the edges of the melt tracks. After the instrument selects the preferred track outline, they were manually checked and corrected. Five such measurements were performed on each track line at different locations. In cases of balling, the track widths are often not consistent, thereby leading to large standard deviation. After the track width measurements, a snapshot of the single-track was stored. The single-tracks were then cut using a low speed saw at the centre of the tracks. The cut samples were embedded, polished and etched.

4. Results

4.1. Single-tracks

Figure 5 below shows single-track samples of varying power, scan speed and duty cycle. Increasing the power and duty cycle tends to increase the track width while increasing the speed reduces the width. Increasing the power to 250 W at lower speed such as 110 mm/s leads to very wide melt tracks and overheating. Whereas decreasing the power to 150 W at higher speed such as 390 mm/s leads to balling.

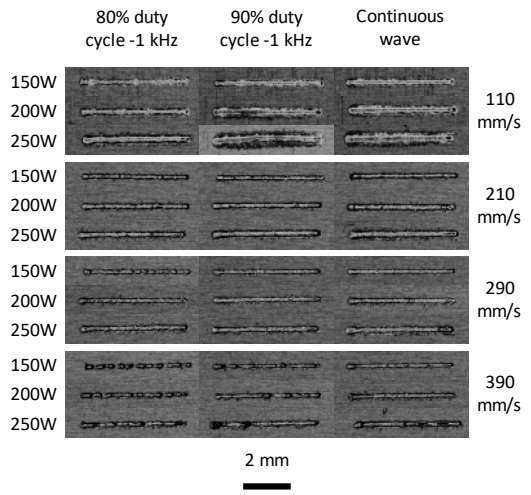

Figure 5. Effect of power, scan speed and duty cycle on single-tracks

Figure 6 shows the beam track widths as a function of the line energy density (LED) defined as the ratio between effective power and scan speed where effective power is the product of the duty cycle fraction and the power. The optimal LED range according to literature for SS316L is between 0.7 to 1.3 J/mm [10]. For pulsed single-tracks the range seems to be similar. There is however, a variability in track width of samples processed using the same parameters. A further analysis showed that on a given plate the set of tracks that are processed second tend to have a larger track width especially at a higher LED. These results are consistent with thermal lensing effects. The thermal lensing could be from the mirrors or the F-θ lens.

Figure 7 shows the change in melt track shape with pulsing and laser power. At lower power like 100 W, the depth of penetration into the base is insufficient although the width may be small. At lower duty cycle like 80%, the depth of penetration and track width are consistently lower while the track height is often higher. In contrast, at duty cycle 90% and at power greater than 150 W, all meltpool parameters are lower in comparison to CW. These results indicate that the trends in pulsed melt track shapes depend on the energy density.

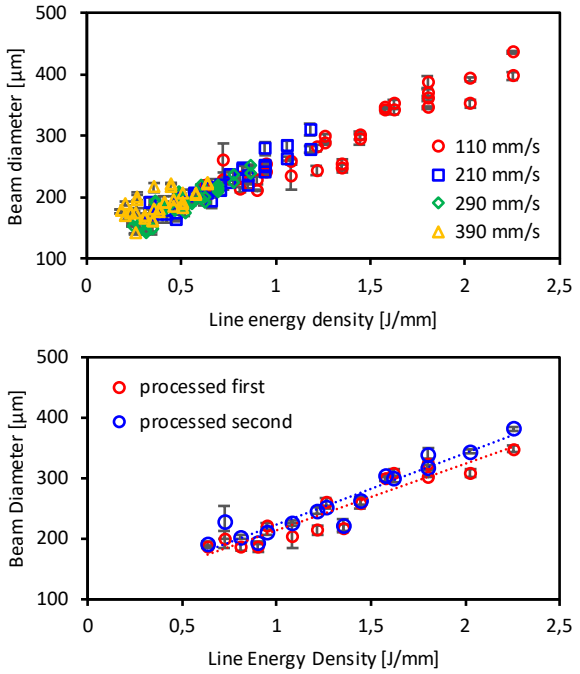

Figure 6. Track width as a function of line energy density on the top, the effect of thermal lensing on track width in the bottom

Figure 7. Effect of laser power and pulsing on melt track shape processed at speed = 210 mm/s

4.2. Photodiode data analysis

Process data acquired at 100 kHz generates 1 GB of data every two minutes. Storing and processing the entire raw data set becomes more complex as the component dimensions increase. Hence, solutions that are developed for a single layer on an open architecture system must be scalable in order to be useful. In this preliminary study, the focus was on the off-axial IR sensor.

The photodiode data could be used to track the intensity of the emissions from the meltpool which correspond to the meltpool area. In the case of the short single-tracks presented in the previous section, balling and meltpool breakdown behaviour was readily observed. From a practical standpoint however, it is important to observe defects while using "good parameters''. Hence, the following section presents results from 40 mm long scan tracks that had occasional meltpool breakdown. The process parameters were chosen such that all of them are expected to have reasonable quality without balling or overheating as shown in Figure 4.

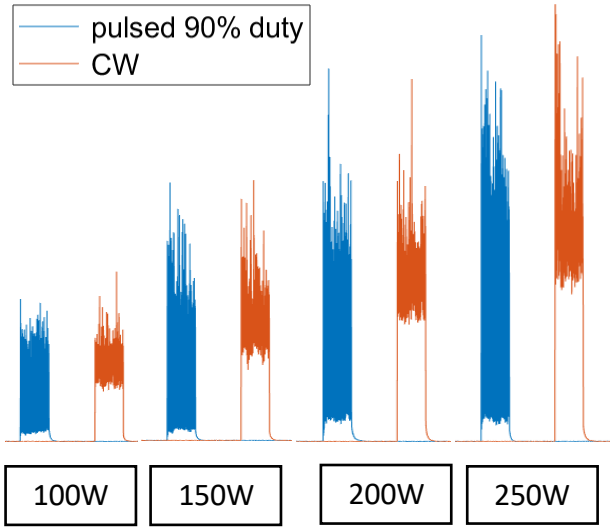

Figure 8. Schematic of single-tracks categorised through visual inspection. Power [W] along Y-axis and duty cycle [%] along X-axis

Figure 8 shows pulsed and continuous wave photodiode signals processed at varying powers at a constant speed of 210 mm/s. The first observable trend is the increase in the average intensity with the increasing power. In pulsed mode, the lower and higher thresholds for the intensity oscillate much more compared to the CW mode. This is because the laser is turned off and on thereby leading to a decrease in meltpool intensity.

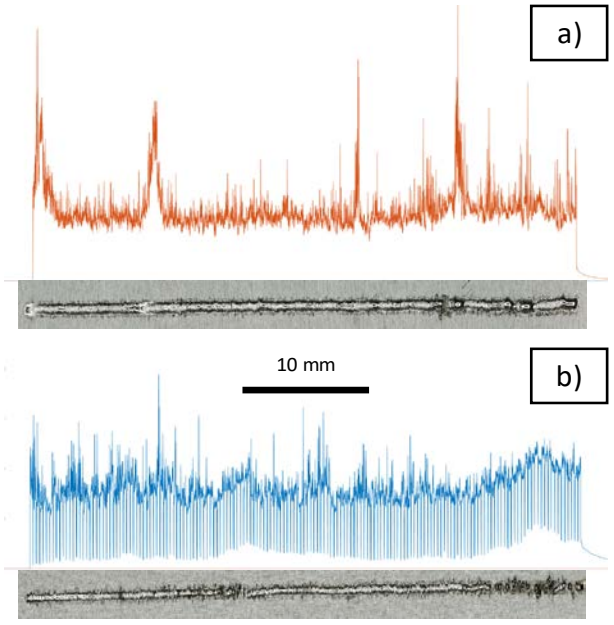

Figure 9. Defect identification using off-axial IR sensor in a) CW on the top and b) pulsed mode L-PBF on the bottom. Both samples were made at 200 W and speed of 210 mm/s

Figure 9 shows the defect identification capabilities of the IR sensor in continuous and pulsed mode of operation. In the case of the CW track, there is a low frequency IR peak at around one-third the track length that corresponds to a break down of the meltpool. Further higher frequency peaks also correspond to spatter or breakdown of the meltpool. In case of pulsed mode, balling is accompanied by a rise in the lower threshold of the intensity. This is due to the breakdown of one continuous meltpool into several thus leading to a higher remnant intensity when the laser switches off. These examples demonstrate the difference in defect indication between pulsed and continuous mode of operation.

5. Conclusions and future work

A photodiode based in-situ sensor module was setup on an open architecture L-PBF system. The light intensity along with the position of the galvo mirrors were acquired at 100 kHz allowing the conversion of time series data into spatial coordinates. Co-axial and off-axial sensors with varying filters and focus optics were tested. Co-axial sensors were found to be highly sensitive to alignment, position and optical filters. Off-axial sensors had a repeatable positional dependence and had a much larger viewing area making them more robust in identifying large defects. A potential solution to improve the co-axial sensor setup is to use transmittive dichroic beam splitters coupled with chromatic aberration corrected focus optics instead of reflective beam splitters.

A set of single-track samples with varying duty cycle, power and speed were made. Thermal lensing effects were identified within each set of single-track samples as evidenced by track width widening. The thermal lensing affected the signals at the co-axial sensors but not the off-axial sensors. Off-axial photodiode data was analysed for varying combinations of single-tracks on-plate versus with powder. The threshold limits for defect indications were different for pulsed mode versus the CW mode. It is imperative to use the robustness of off-axial sensors coupled with the sensitivity of the co-axial sensors to develop quality metrics for certification and feedback control of pulsed mode L-PBF.

References

[1] Everton, S. K., Hirsch, M., Stravroulakis, P., Leach, R. K., & Clare, A. T. 2016 *Materials & Design* **95** 431-445

[2] Grasso, M., & Colosimo, B. M. 2017 *Meas. Sci. & Tech.* **28** 044005.

[3] You, D. Y., Gao, X. D., & Katayama, S. 2014 *Sci. & tech. of welding & joining* **19** 181-201

[4] Craeghs, T., Bechmann, F., Berumen, S., & Kruth, J. P. 2010 *Phys. Proc.* **5** 505-514

[5] Clijsters, S., Craeghs, T., Buls, S., Kempen, K., & Kruth, J. P. 2014 *The Int. J. of Adv. Man. Tech.* **75** 1089-1101

[6] Craeghs, T., Clijsters, S., Kruth, J. P., Bechmann, F., & Ebert, M. C. 2012 *Physics Procedia* **39** 753-759

[7] Demir, A. G., De Giorgi, C., & Previtali, B. 2018 *J. of Man. Sci. & Eng.* **140** 041003

[8] Demir, A. G., Mazzoleni, L., Caprio, L., Pacher, M., & Previtali, B. 2019 *Optics & Laser Technology* **113** 15-26

[9] Doubenskaia, M., Grigoriev, S., Zhirnov, I., & Smurov, I. 2016 *Rapid Prototyping Journal* **22** 40-50

[10] Kamath, C., El-dasher, B., Gallegos, G. F., King, W. E., & Sisto, A. 2014 *The Int. J. of Adv. Man. Tech.* **74** 65-78